JVST A
Journal of Vacuum Science & Technology A

ARTICLE

avs.scitation.org/journal/jva

Effects of structured electrodes on electron power absorption and plasma uniformity in capacitive RF discharges

Cite as: J. Vac. Sci. Technol. A 39, 063004 (2021); doi: 10.1116/6.0001327
Submitted: 2 August 2021 · Accepted: 6 October 2021 ·
Published Online: 26 October 2021

Li Wang,[1,2] Peter Hartmann,[3] Zoltán Donkó,[3] Yuan-Hong Song,[1,a)] and Julian Schulze[1,2]

AFFILIATIONS

[1]Key Laboratory of Materials Modification by Laser, Ion, and Electron Beams (Ministry of Education), School of Physics, Dalian University of Technology, Dalian 116024, People's Republic of China
[2]Department of Electrical Engineering and Information Science, Ruhr-University Bochum, D-44780 Bochum, Germany
[3]Institute for Solid State Physics and Optics, Wigner Research Centre for Physics, Konkoly-Thege Miklós str. 29-33, H-1121 Budapest, Hungary

[a)]**Electronic mail:** songyh@dlut.edu.cn

ABSTRACT

The electron power absorption dynamics and plasma uniformity in low pressure capacitively coupled RF discharges with structured electrodes are investigated by graphics processing unit-based 2d3v particle-in-cell/Monte Carlo simulations in argon gas. In the presence of planar electrodes, the plasma is radially nonuniform due to strong electron density peaks close to the reactor sidewall, which are caused by edge effects that locally enhance the electron power absorption and ionization. Such a local enhancement of these characteristics can also be achieved in a controllable manner by using a single ring-shaped rectangular trench embedded in the powered electrode close to the reactor center. This effect is understood by analyzing the trajectories of selected electrons as well as the time evolution of their energy and velocity inside and above such trenches. Electrons are found to gain high energies inside the trench by bouncing between the sheaths at the trench walls during the sheath expansion phase. Combined with the cross-firing of energetic electrons at the trench orifice, this leads to high local ionization rates. Using these trench effects, the plasma uniformity above the wafer placed on a planar powered electrode can be remarkably improved by including multiple trenches in the opposing grounded electrode, which enhance the ionization and plasma density at their respective radial positions. Meanwhile, the ion flux-energy distribution function at the wafer is found to be almost unaffected.

I. INTRODUCTION

Capacitively coupled plasma (CCP) sources have been widely used in the microelectronics industry due to their simple geometry and ability to generate large area plasmas. Common applications including dry etching, plasma enhanced chemical vapor deposition (PECVD), and sputtering require controllable ion flux-energy distribution functions at the dielectric wafer to achieve ideal processing performance.[1–3] Typical CCPs are generated between two parallel-plate electrodes separated by a small distance in a vacuum reactor. Different methods have been proposed in the past years to enhance the control of plasma properties in such systems. For instance, utilization of very high driving frequencies is found to significantly enhance the plasma density.[1–4] Independent control of ion flux and energy can be realized via the electrical asymmetry effect (EAE),[5–15] and control of electron power absorption and energy distributions is possible via adjusting the sheath dynamics by using tailored voltage waveforms (TVWs).[16–27] With a magnetic field applied to the system, the plasma density is found to be increased due to enhanced electron power absorption and reduced electron energy loss at the boundary surfaces.[28–34]

Although improved plasma properties can be realized by using these methods, significant problems still exist; plasma nonuniformity is usually observed in CCP discharges at various conditions. With a very high driving frequency applied, the electromagnetic wavelength in the plasma is comparable to the CCP reactor diameter. Thus, electromagnetic effects, such as the standing wave[35–39]

and the skin effect,[40,41] become evident and lead to nonuniform plasma densities in the radial direction. In addition, the electrostatic edge effect is found to cause higher densities near the reactor sidewall compared to the density near the discharge center due to the intensive ionization near the edges.[42–44] The development of large area, high density, and uniform CCP sources is to be accomplished.

This requires finding ways to locally control the electron power absorption in radial direction over the wafer surface. Hollow cathode (HC) discharges might help us to achieve this goal. They consist of a direct current (DC) or radio frequency (RF) driven hollow cylindrical or rectangular electrode (with a hole diameter of typically several millimeters) and a grounded counter electrode. Such HC plasmas have been widely used in a number of applications, such as light sources, ion lasers, spacecraft propulsion as well as etching, and deposition devices due to their ability to generate high density plasmas.[45–48] In such plasma sources, energetic electrons are confined within the cavity and oscillate between the sheaths at the HC walls (pendular motion),[49] which is called the hollow cathode effect (HCE). In this way, such electrons are confined well, generate strong ionization, and, therefore, enhance the plasma density.[45]

Previous studies have shown that utilization of the HCE in large area CCP discharges by using structured electrodes can enhance the plasma density and improve plasma uniformity.[50–53] For instance, an enhanced deposition rate was found to be realized experimentally by using a multihollow electrode to generate a high density CF_4 plasma.[54] Using a single ring-shaped powered electrode, Ohtsu and Fujita demonstrated that the plasma density profile can be modified by the HCE, while the HCE will only occur, if the trench width is approximately equal to the sum of the electron mean free path and twice the sheath thickness so that the plasma can penetrate into the structures.[55] They also found that the effect of the hollow trench varies as a function of the trench shape and depth.[56,57] Moreover, the plasma density was found to be 1.5–3 times higher in the presence of strong secondary electron emission (SEEs) at the cathode.[58] The importance of SEE for the HCE is also reported by Lafleur and Boswell in Ref. 59, where a HC discharge within a multislit electrode was found to be sustained only in the presence of SEE at the discharge conditions studied by particle-in-cell/Monte Carlo collision (PIC/MCC) simulations. Schmidt *et al.* studied the effect of various structured electrode topologies on CCP discharges experimentally.[60] They found a local agglomeration of energetic electrons above the trenches, which modifies the ionization and plasma density profiles.

Although previous investigations have shown that setting trenches at the powered electrode can enhance the plasma density and improve the plasma uniformity to some extent in CCP discharges, the fundamental understanding of these effects is still limited. In particular, the effects of such electrode structures on the electron power absorptions dynamics are unclear. This includes the energy gain process of cold bulk electrons that penetrate into the trench and their interactions with the sheaths at the trench walls. Understanding these processes is important for the knowledge-based design of structured electrodes to improve plasma properties. It requires tracing the electrons' motion and the temporal evolution of their energy inside the trench. Based on such fundamental understanding, further investigations are needed to explore whether a sufficiently uniform plasma can be realized above planar wafers in realistic reactor geometries at low pressure by structuring the counter electrode. Such studies can only be realized by 2d3v PIC/MCC simulations, since a kinetic treatment of electrons is required under such process conditions and realistic chamber geometries must be considered including the geometric reactor asymmetry. Such simulations allow testing various reactor and electrode designs prior to realizing them experimentally, which is expensive and time consuming.

In this work, we conduct such studies in a geometrically asymmetric CCP reactor by using a 2d3v Graphics Processing Unit (GPU) accelerated PIC/MCC code in argon gas at low pressure. First, the electron power absorption dynamics is studied without and with a trench implemented in the powered electrode. In the latter case, we trace the electrons' motion inside a trench and find a high electron mean energy inside the trench as a consequence of electron bounce resonance heating between the sheaths at the sidewalls of the trench.[61] Cross-firing of energetic electrons at the trench orifice leads to a high ionization rate above the trench and greatly enhances the local plasma density. Based on this, we set different numbers of trenches at the grounded electrode to compensate the radial nonuniformity of the plasma density in the vicinity of the powered electrode, which is caused by the high density peaks at the radial electrode edges in the presence of planar electrodes. In this way, the plasma uniformity above the wafer is demonstrated to be improved significantly. The paper is structured in the following way: the 2d3v PIC/MCC simulation is described in Sec. II including the definition of the electrode configurations studied. The effects of trenches on the electron power absorption dynamics and the radial plasma uniformity are studied in Sec. III. Finally, concluding remarks are given in Sec. IV.

II. PIC/MCC SIMULATION

A. PIC/MCC code and basic simulation parameters

The argon discharges studied here are described by a cylindrical 2d3v (two-dimensional in space and three-dimensional in velocity space) electrostatic PIC/MCC code. While azimuthal symmetry is assumed, the radial and axial directions are resolved. A detailed introduction of this code including grid settings and the Poisson solver can be found in our previous works.[62,63] The reactor geometries studied in this work are shown in Fig. 1, the plasma is generated between the top electrode (blue solid line) being grounded and the bottom electrode (red solid line) being driven by a single-frequency voltage waveform, $V = V_0 \cos(2\pi ft)$. The diameter and gap distance of the chamber are 24 and 3 cm, respectively. As indicated by the light blue line, a dielectric spacer having a width of 2.3 mm is set between the two electrodes. Such a spacer corresponds to either a dielectric or a thin gap in experiments. A linear drop of the potential across it is assumed when solving the Poisson equation. Due to the small dimension of the dielectric spacer, its impact on the discharge is not significant. Although commercial CCP reactors sometimes have more complicated geometries including side flanges and gas/plasma volumes in between the radial electrode edges and the sidewalls, the geometry studied in this work is, in fact, used for experiments and industrial

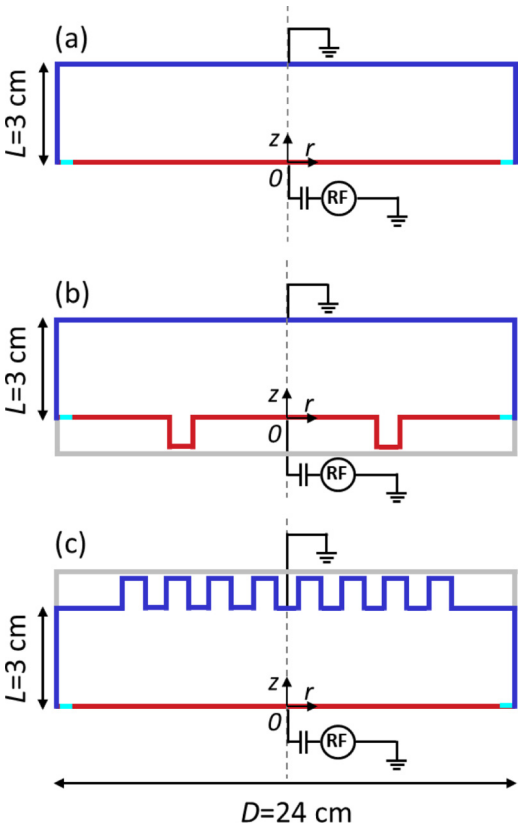

FIG. 1. Reactor geometries investigated: (a) planar electrodes, (b) planar grounded electrode and structured powered electrode including a single ring-shaped rectangular trench, and (c) planar powered electrode and structured grounded electrode including multiple trenches. The bottom powered electrode is indicated by the red line and the top grounded electrode is indicated by the dark blue line. The light blue segments in between the powered and grounded electrodes represent a dielectric spacer.

applications[8,64,65] and provides important general insights into the discharge characteristics in geometrically asymmetric systems.

The effects of different trench dimensions and shapes on the plasma characteristics, which are expected to vary as a function of discharge conditions, are not studied in this work, but represent an important topic for future investigations. Here, we focus on the fundamental understanding of the effects of structured electrodes on the electron power absorption dynamics and plasma properties for the following specific discharge conditions: argon gas at a pressure of $p = 10$ Pa, gas temperature of $T = 400$ K, driving frequency of $f = 13.56$ MHz, and driving voltage amplitude of $V_0 = 300$ V. Although secondary electrons are reported to be important to sustain the discharge at some conditions,[59] secondary electron emission and electron reflection at the boundaries are found not to dramatically change the effects of the trenches under the discharge conditions studied here. Therefore, such effects are neglected in this work.

We trace electrons and Ar^+ ions in the simulations. Electron–Ar atom collisions include elastic scattering, excitation into 25 individual levels and ionization;[66–69] Ar^+–Ar collisions include elastic [isotropic and backward (charge exchange)] scattering and excitation into three individual levels.[70,71] More detailed information concerning the treatment of the collision processes and the cross sections can be found in Refs. 16 and 72–74. In the simulations, 1024 grid points in the radial and axial directions are used to resolve the Debye-length. Particles are traced with 30 000 time steps per RF period to provide sufficiently accurate computations of the electron trajectories and to fulfill all stability criteria of the simulation. The number of superparticles ranges between 7×10^6 and 1×10^7.

B. Implementation of trenches

To study the effect of the trenches, several different chamber geometries are studied, as shown in Fig. 1, i.e., a geometry based on planar powered and grounded electrodes (a), a scenario based on a planar grounded electrode and a structured powered electrode including a single ring-shaped rectangular trench (b), and a case with a planar powered electrode and a structured grounded electrode including multiple trenches (c). To find a good configuration for improving the plasma uniformity at the wafer, the effects of different numbers of trenches at the grounded electrode are studied in scenario (c). Figure 1(c) shows the example case with four ring-shaped rectangular trenches at the grounded electrode. The trench boundaries are considered as a part of the electrodes in the simulations i.e., these have the same potential as the powered/grounded electrode. Considering these boundary conditions, the potentials in the whole chamber (including the potentials in the trench) are obtained by solving the Poisson equation.[62,63] In this work, we first study the plasma properties in the chamber shown in Fig. 1(a) in the presence of planar electrodes. Based on this, the effects of hollow electrodes on the electron power absorption dynamics and plasma uniformity are investigated by setting trenches at the powered/grounded electrode. Although different positions and numbers of the trenches are studied, we fix the shape and dimension of each trench. We study the effects of one/multiple ring-shaped rectangular trench(es) at the electrodes with a trench depth of $d = 1$ cm and width of $w = 1$ cm/$w = 1.5$ cm. Based on several tests, these trench dimensions are chosen to ensure that electrons penetrate into the structures during the local sheath collapse. If the trench dimensions are too small, this will not happen and there is very little effect of such trenches on the plasma.[55,56] Using too large trench dimensions also results in reduced effects on local plasma properties in the vicinity of the structures.

III. RESULTS

A. Electron heating dynamics in the vicinity of trenches

For the reactor geometries studied in this work (see Fig. 1), a large sheath is formed at the powered electrode due to the geometrical asymmetry. In order to maximize the effect of the trench on the plasma density, we first set a ring-shaped trench at the powered electrode to get a fundamental understanding of its effects on the electron power absorption dynamics. Figure 2 shows the 2D space-resolved and time-averaged electron density in the chamber for the

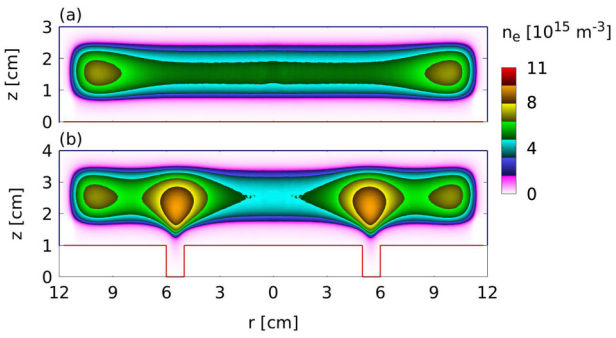

FIG. 2. 2D spatial distributions of the time-averaged electron density in the presence of planar electrodes (a) and with a single ring-shaped rectangular trench at the powered electrode located at $r = 5.5$ cm with a trench width of $w = 1$ cm and a depth of $d = 1$ cm (b). Discharge conditions: Ar, 10 Pa, $f = 13.56$ MHz, $V_0 = 300$ V, 3 cm electrode gap, 24 cm electrode diameter, and 400 K gas temperature.

case of planar electrodes (a) and in the presence of a ring-shaped trench at the powered electrode with a width of $w = 1$ cm and a depth of $d = 1$ cm (b). High density peaks are observed near the sidewalls in both cases. These are caused by the strong ionization near the sidewall due to the edge effect. With a hollow powered electrode, the electron density above the trench is found to be enhanced strongly. As a consequence, the local plasma density above the trench is higher than the density near the sidewalls.

In order to provide insight into the formation of the spatial distribution of the plasma density, Figs. 3 and 4 show the spatial distributions of the ionization rate at eight different times within one RF period in the presence of planar electrodes and with a trench at the powered electrode, respectively. Since the system is azimuthally symmetric, only the results in the right half of the reactor are shown. Due to the geometrical asymmetry, a negative DC self-bias of −77.6 V is generated in the planar electrode scenario, which leads to a large sheath at the powered electrode. Strong electron power absorption and ionization are observed during its expanding phase as shown in Fig. 3(c). A smaller sheath is formed at the grounded electrode, for which the ionization rate near the planar part of the grounded electrode is lower. However, a very strong ionization peak is formed at the top right corner of the chamber during the sheath expansion at the grounded electrode, as shown in Fig. 3(g). This intensive ionization is caused by the superposition of a vertically (at the top electrode) and a horizontally (at the sidewall) expanding sheath near the "corner," which greatly enhances the electron heating.

It is found that ionization peaks are also formed near the bottom right corner during the sheath expansion at the powered electrode, as shown in Figs. 3(b)–3(d). However, the ionization here is lower compared to that at the top-right corner during the local sheath expansion phase, since the sheaths at this corner move toward different directions, i.e., the sheath at the sidewall collapses during the sheath expansion at the bottom electrode. In contrast to very low gas pressure cases, where nonlocal effects are important and the enhanced electron power absorption at the corners leads to the generation of energetic electron beams that can propagate far toward the chamber center resulting in a center-high density profile,[62] here the strong electron heating at the corners leads to more local peaks of the ionization rate and of the plasma density near the edges at the higher of $p = 10$ Pa.

With the presence of a trench at the powered electrode, the ionization dynamics change markedly. While ionization peaks at the corners of the reactor still exist, which keep the density high near the sidewall, additional ionization peaks are observed above the trench as a result of the enhanced electron power absorption inside and above this structure. The trench enlarges the surface area of the powered electrode compared to the planar electrode case. Thus, the DC self-bias is reduced to −59.6 eV. A large sheath is still formed at the powered electrode. During its expanding phase, a high ionization rate is initially observed inside the trench

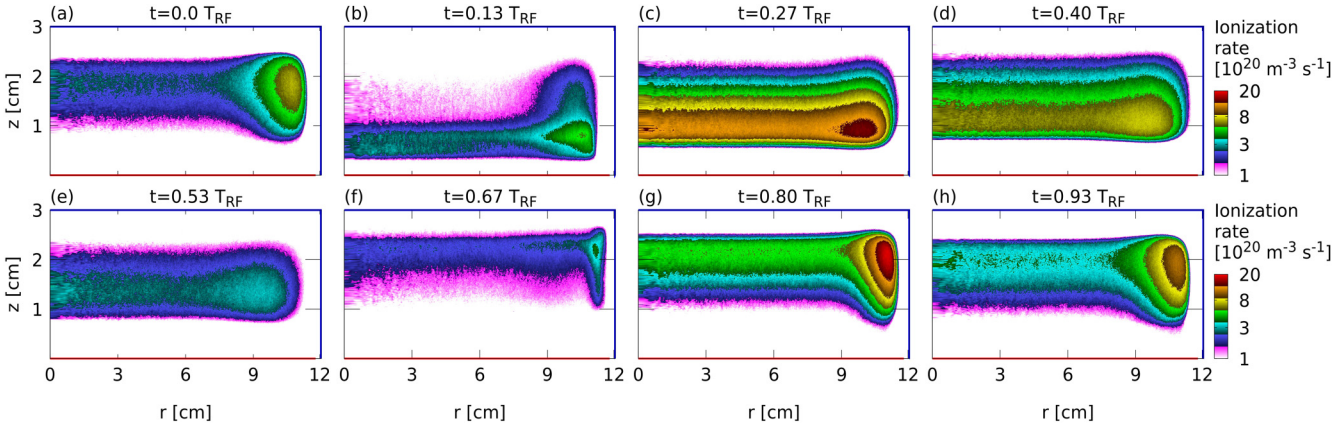

FIG. 3. 2D spatial distributions of the ionization rate at eight different times (a)–(h) within one RF period in the presence of planar electrodes. The discharge conditions are the same as in Fig. 2. Since the chamber is azimuthally symmetric, only the results for the right half of the cross section of the reactor are shown.

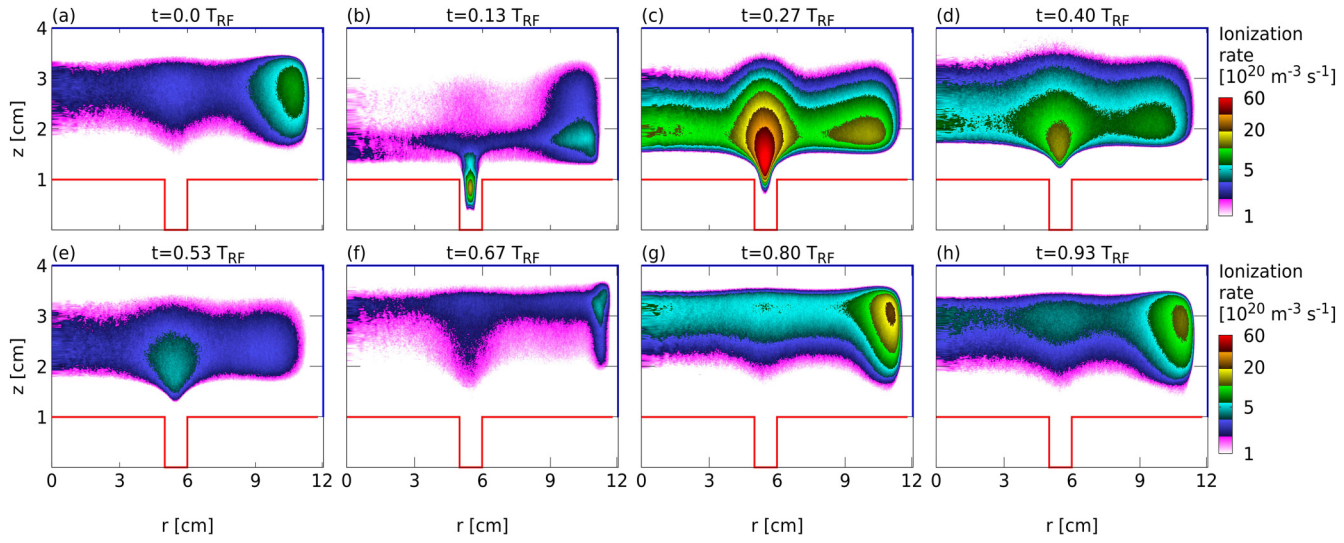

FIG. 4. 2D spatial distributions of the total ionization rate at 8 different times (a)–(h) within one RF period in the presence of a single ring-shaped trench at the powered electrode. The other discharge conditions are the same as in Fig. 2.

at $t = 0.13\ T_{RF}$, and then extremely strong ionization is found above the trench orifice, as shown in Figs. 4(b)–4(e). These simulation results are in excellent agreement with previous experimental findings of Schmidt *et al.*,[60] which verify our computational results. Such a strong local ionization at a specific radial position modifies the radial plasma density profile, i.e., a high density is observed above the trench, as shown in Fig. 2.

In order to understand these effects of the trench on the ionization and the plasma density inside and above the structure, Fig. 5 shows the axially and radially resolved electric field E_z and E_r, the mean electron energy, and the ionization rate near the trench at four different times during the sheath expansion phase at the powered electrode. At $t/T_{rf} = 0$, the local sheath is fully collapsed, the electric field inside the trench is weakest in both the radial and axial directions. Thus, electrons can penetrate into the trench. When the sheath starts to expand, the electric field in the trench gradually builds up, the electrons in the trench are accelerated strongly by the electric field, which leads to a high mean electron energy and ionization rates inside the trench, as shown in the second and third columns of the figure. According to Figs. 5(c2) to 5(c4), the mean electron energy in the trench is enhanced evidently. As illustrated in detail in the following, this is caused by electron bounce resonance heating between the sheaths at the trench walls, i.e., the sheaths at the trench sidewalls expand toward each other in radial direction so that electrons are accelerated resonantly back and forth between these lateral sheaths. With the sheath further expanding, a strong electric field is found everywhere inside the trench so that electrons are accelerated out of the trench through its orifice and into the plasma bulk. At the corners of the trench orifice the sheath edge is curved and, thus, its expansion velocity vector has radial as well as axial components. Consequently, a cross-firing of highly energetic electrons at the orifice of the trench happens. In combination with the energetic electrons being pushed out of the trench, this leads to a high local ionization rate, as shown in Fig. 5(d4). Previous experimental studies by Schmidt *et al.*[60] proved that a ring-shaped trench having a width of 1 cm can effectively modify the plasma density in a neon discharge at similar discharge conditions as used in our work: driving frequency 13.56 MHz, voltage amplitude 264 V, gas pressure 10–20 Pa. In agreement with our simulation results, this was found to occur due to a local increase of the electron power absorption above the trench orifice. Lee *et al.*[51] also reported that the plasma density enhancement is most pronounced by setting a multihole electrode with a hole diameter 1 cm at a gas pressure of 64.5 mTorr and a driving frequency of 13.56 MHz in a large voltage range in an argon discharge. At $t = 0.27\ T_{RF}$, the sheath is almost fully expanded, most of the electrons have left the trench. Thus, no more ionization is observed inside the structure. In contrast to the ionization rate, which is high at the orifice of the trench and low inside the trench at this time, the mean electron energy is high inside the trench in Fig. 5(c4) but much lower above the trench. This is because the electron density is high outside the trench due to a high local density of low energy bulk electrons. In the work of Schmidt *et al.*,[60] high excitation peaks were also observed at the trench corners with a large trench size, i.e., 6.6 cm trench width and 6 cm trench depth, which is caused by edge effects similar to the ones we observed at the chamber corners in Figs. 3 and 4. Such effects are absent in Fig. 5 since the trench size is much smaller, the electrons in the whole trench can be strongly heated during the sheath expansion, which makes the electron heating enhancement at the corners to be not evident.

The above explanations can further be supported by the observation of the trajectories of individual electrons within the trench. Figure 6 shows such an exemplary trajectory during the local sheath expansion phase as well as the variation of the energy, axial and radial velocity components of this sample electron as a

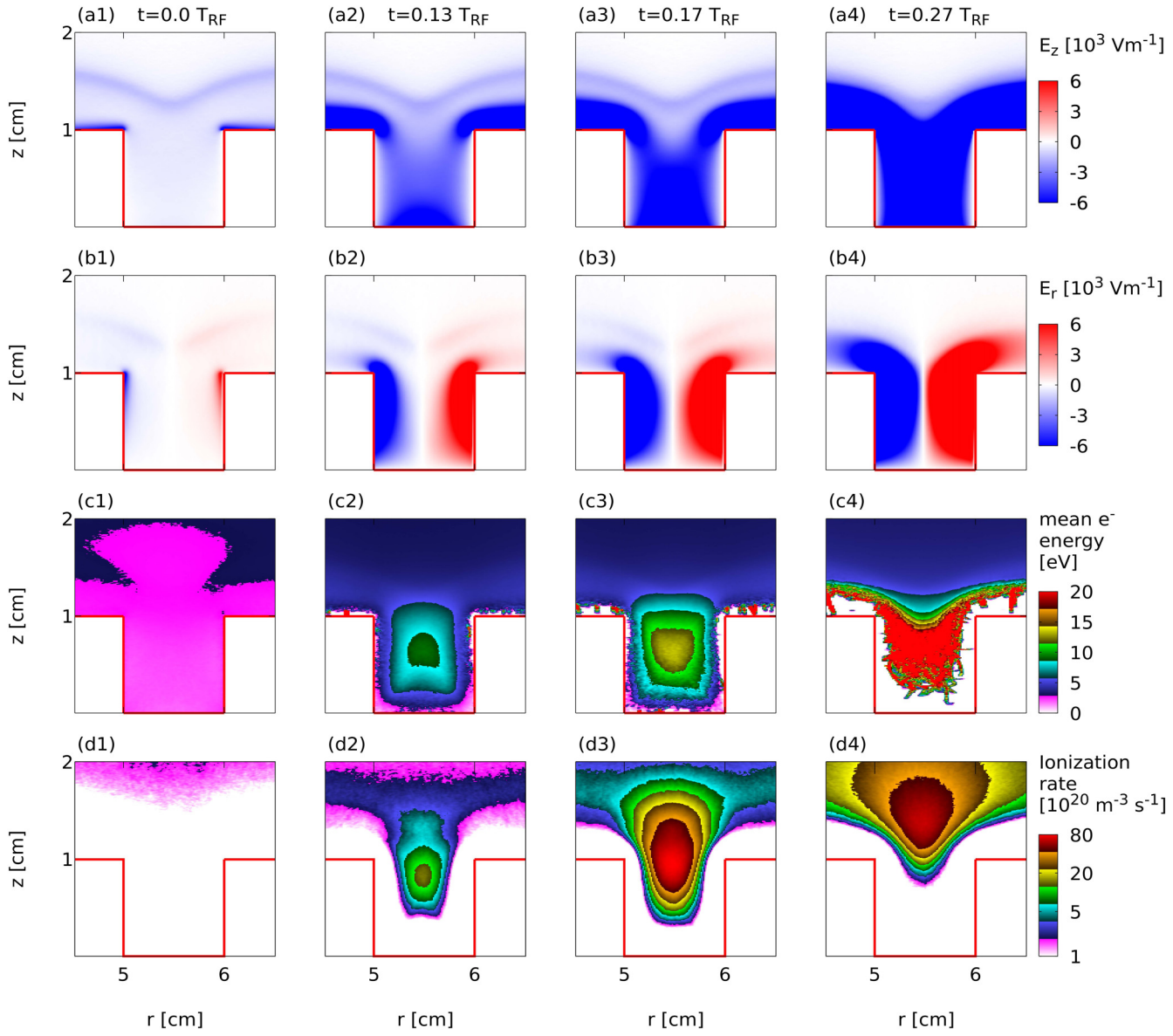

FIG. 5. 2D spatial distributions of the electric field in the axial direction E_z (a1)–(a4), the electric field in the radial direction E_r (b1)–(b4), the mean electron energy (c1)–(c4), and the ionization rate (d1)–(d4) near the trench at four different times during the sheath expansion phase at the powered electrode within one RF period: $t/T_{rf} = 0$ (first column), $t = 0.13\ T_{RF}$ (second column), $t = 0.17\ T_{RF}$ (third column), and $t = 0.27\ T_{RF}$ (fourth column). The other discharge conditions are the same as in Fig. 2.

function of time starting from $t/T_{rf} = 0$ when the sheath at the powered electrode starts to expand. According to Fig. 6(a), the electron initially moves toward the bottom center of the trench. It is reflected by the bottom sheath at point "1" and point "2" where its axial velocity reaches 0 as shown in Fig. 6(c). The knee point in between the red and the green points is caused by a collision, which reverses the axial velocity direction of the electron. Soon after point "2," the electron is reflected by the expanding sheath at the right sidewall. Thus, its energy continuously increases until point "3," where an inelastic collision occurs. At points "4," "5," and "6," three more collisions occur. The radial velocity of the electron changes direction at point "5," where it has already entered the sheath at the left sidewall. The radial velocity first increases then decreases from point "5" to point "7" as the electron moves toward the right sidewall, since it is accelerated initially by the expanding sheath at the left sidewall and then decelerated, when it

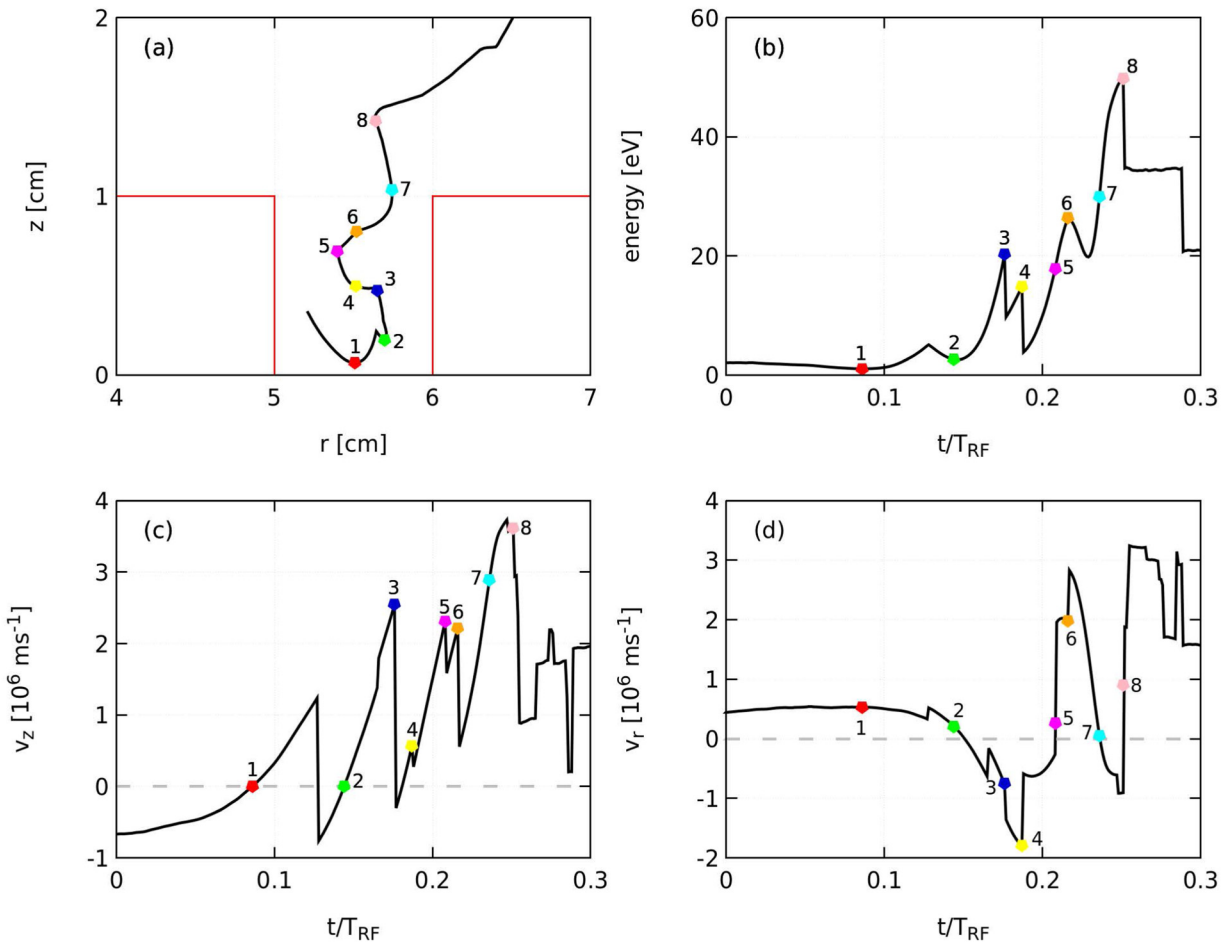

FIG. 6. Trajectory of an electron inside the trench during the local sheath expansion phase (a) and the time evolution of its energy (b), of its axial velocity (c), and of its radial velocity component (d). The discharge conditions are the same as in Fig. 2. The numbers assist cross-referencing between the different panels.

penetrates into the sheath at the right sidewall. At point "7," the electron is reflected by the expanding sheath at the right sidewall. Thus, its energy continuously increases and reaches around 53 eV at point "8," since it is accelerated by both the vertical sheath at the trench bottom and the horizontal sheath at the right sidewall. After point "8," the electron leaves the trench region. This analysis of the motion of a single electron is representative of the dynamics of electrons in the trench region during the phase of local sheath expansion. Overall, electrons penetrate into the trench during the local sheath collapse and are then accelerated to high energies by electron bounce resonance heating inside the trench, during which both, the sheaths at the trench sidewalls and the sheath at the trench bottom, play important roles for the electron power absorption.

Originally, this effect was discovered in planar CCPs driven at particular frequencies and with particular electrode gaps at low pressure,[61] where electrons accelerated by sheath expansion heating at one electrode propagate toward the bulk collisionlessly and arrive at the opposite electrode, when the local sheath is expanding, so that they gain additional energy upon reflection by this sheath. In the scenario studied here, the sheaths adjacent to the trench walls expand simultaneously so that electron bounce resonance heating always occurs inside the trench. While bouncing between these sheaths, such electrons cause ionization inside the trench and finally leave the trench with high energies, which allows them to cause ionization outside the structure as well. The cross-firing of these energetic electrons at the orifice of the trench leads to a strong local ionization peak above the trench, as shown in Fig. 5(d4).

It is also worth noting that the electron bounce resonance heating happens only in the trenches with appropriate sizes. Based on previous studies[50,51,75] and several tests we made by simulations, the trench width should be larger than twice the sheath width. For a smaller trench width, the bulk electrons can hardly penetrate into the trench, no significant electron heating can occur within the trench. If the trench width is too large, i.e., much larger than twice the sheath width, the trench effect would also decrease, which has also been examined by experiments previously.[51,55] Based on Fig. 6,

we can estimate the maximum trench width for the occurrence of electron bounce resonance in the trench. From Fig. 6, the electron is found to leave the trench at point 7, which means that from $t = 0$, i.e., when the electron starts to be accelerated in the trench, the electron residence time in the trench is around 0.25 T_{RF}, i.e., 18.4 ns. This is mainly determined by the depth of the electron penetration into the trench and the axial velocity which is related to the electron acceleration in the vertical sheath. Based on Fig. 6(d), we use a radial electron velocity $v_r = 1 \times 10^6$ m/s to estimate the distance that the electron can travel in the radial direction within its residence time in the trench. By multiplying with the time, this distance is 1.84 cm; if the trench width is larger than this value, the electron that starts near one of the trench walls would leave the trench before it can reach the opposite sheath and bounce back. This is also coincident with the findings of Ref. 50, where based on the experimental results, the authors suggest the hole diameter to be three to five times the sheath width to achieve a strong effect of the structured electrode. At the discharge conditions studied in our work, the time-averaged sheath width at the trench wall is around 0.37 cm for the trench at the powered electrode and around 0.32 cm for the trench at the grounded electrode. Therefore, significant electron bounce resonance heating is observed.

B. Plasma uniformity improvement with customized boundary surface topologies

Through the above analysis, the trench at the powered electrode is found to greatly change the electron power absorption dynamics and to modify the radial plasma density profile. Such trench effects are promising to improve the radial plasma uniformity at a planar wafer located on the powered electrode by including trenches at the counter (grounded) electrode. This is of great significance for industrial applications of CCPs. To test this concept, we vary the number of trenches in the grounded electrode. The goal is to find a good configuration of trenches to improve the plasma uniformity at the powered electrode.

Figures 7 and 8 show the spatial distributions of the time-averaged electron density and ionization rate, respectively, for the cases with 1–4 ring-shaped trenches at the grounded electrode. Notice that the trench width in Figs. 7(b) and 7(c) is 1.5 vs 1 cm in (7a) and (7d). This selection is made to ensure that a larger region in the radial direction is affected by each trench to improve radial uniformity in the presence of a low number of trenches. Electron density/ionization peaks are always observed below the trenches due to their effects on the electron power absorption dynamics described above. Since the sheath at the grounded electrode is much smaller compared to the sheath at the powered electrode due to the geometric reactor asymmetry, the electron power absorption inside these trenches via bounce resonance heating is less prominent. Thus, the density/ionization peaks generated below the trenches are lower compared to those formed by the powered electrode trench in Fig. 2(b)/Fig. 4. However, the density peaks generated below the trenches are comparable to the density peaks near the sidewalls of the reactor caused by edge effects. Thus, such trenches can be used to make the plasma more uniform in the radial direction. As shown in Fig. 7(d), the plasma is fairly uniform in the presence of four trenches at the grounded electrode. In Fig. 8, strong ionization is also observed at the opposite sheath at the powered electrode at the radial positions where the trenches are located inside the grounded electrode since a high number of electrons is accelerated toward the powered electrode by the sheath at the trenches, which leads to the ionization peaks near the local sheath edge during the sheath expansion at the powered electrode.

By setting trenches at the grounded electrode, the ionization in the central region of the reactor is enhanced, which leads to an increase of the electron density in the center. Figure 9(a) shows the radial distribution of the time-averaged electron density near the powered electrode ($z = 1$ cm). A good plasma uniformity is found

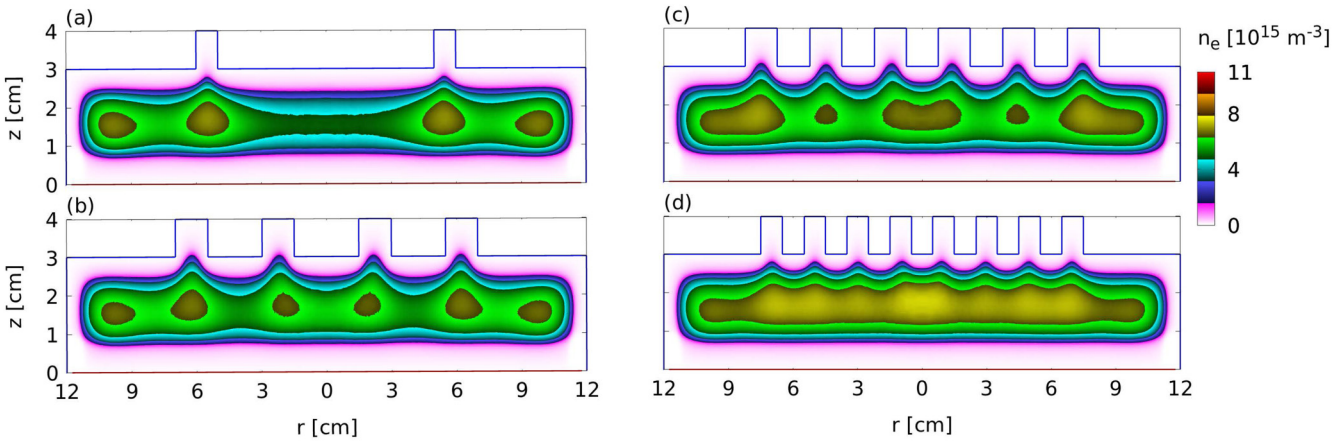

FIG. 7. 2D spatial distributions of the time-averaged electron density for a reactor with ring-shaped trench(es) at the grounded electrode: one trench ($w = 1$ cm, $d = 1$ cm) at $r = 5.5$ cm (a); two trenches ($w = 1.5$ cm, $d = 1$ cm) at $r = 2.25$ cm and $r = 6.25$ cm (b); three trenches ($w = 1.5$ cm, $d = 1$ cm) at $r = 1.5$ cm, $r = 4.5$ cm, and $r = 7.5$ cm (c); and four trenches ($w = 1$ cm, $d = 1$ cm) at $r = 1$ cm, $r = 3$ cm, $r = 5$ cm, and $r = 7$ cm (d).The other discharge conditions are the same as in Fig. 2.

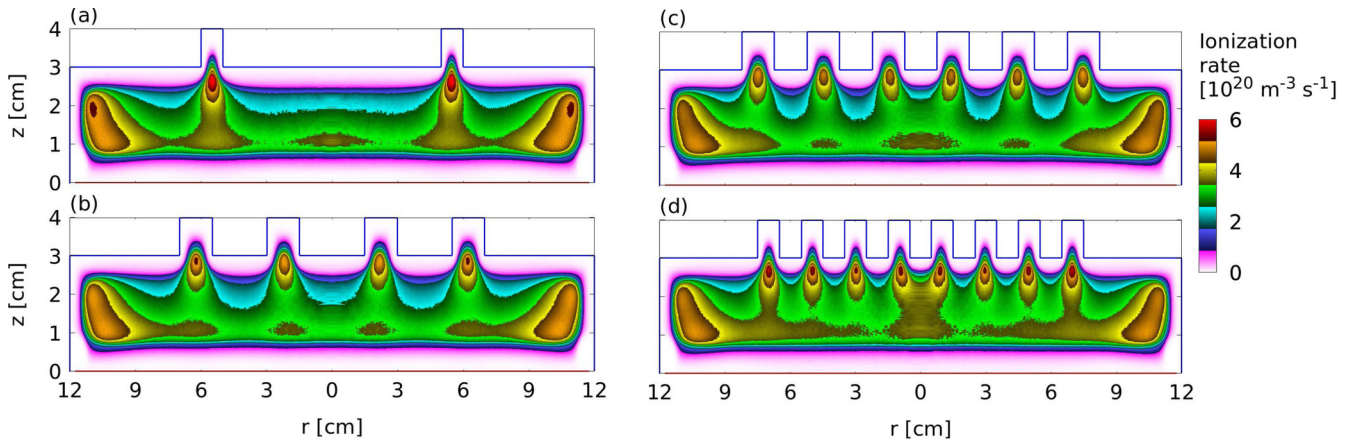

FIG. 8. 2D spatial distributions of the time-averaged ionization rate for reactors with 1–4 ring-shaped trenches [(a)–(d) with sizes and positions specified in Fig. 7] at the grounded electrode. The other discharge conditions are the same as in Fig. 2.

in the presence of four trenches at the grounded electrode, while a poor uniformity is observed in the absence of trenches. The relative nonuniformity ($n_{max}/n_{min} - 1$, where n_{max} and n_{min} are the maximum and minimum electron densities in the bulk region at $z = 1$ cm, respectively) is reduced from 43% (no trench case) to 6% (four trenches case). Moreover, these trenches are found to have only a weak influence on the ion flux-energy distribution function (IFEDF) at the powered electrode, although the DC self-bias changes from −77.6 V (planar electrode) to −96.7 V (four trenches at the grounded electrode) due to the enhanced geometrical asymmetry, as shown in Fig. 9(b).

While different reactor configurations might be used in commercial CCPs, plasma nonuniformity caused by similar edge effects[42,44] always happens. By introducing trenches and adjusting their positions and dimensions, such nonuniformities are expected to be reduced. Radial nonuniformities caused by other effects such as the standing wave and the skin effect are also expected to be reduced in this way. In the case of center-peaked radial density profiles such as those resulting from the standing wave effect, trenches would have to be located close to the electrode edge to enhance the local plasma densities at these positions relative to the electrode center. As long as the neutral pressure is low enough and the electrode gap is small enough, such trenches can be placed at the grounded electrode and will still yield a uniform plasma at the planar wafer, which is located on the powered electrode. In fact, such counter electrodes are typically already structured due to the presence of a showerhead electrode design used for the gas supply. Redesigning the dimensions of the showerhead holes based on predictions of realistic PIC/MCC simulations to enhance plasma uniformity seems to be a promising approach.

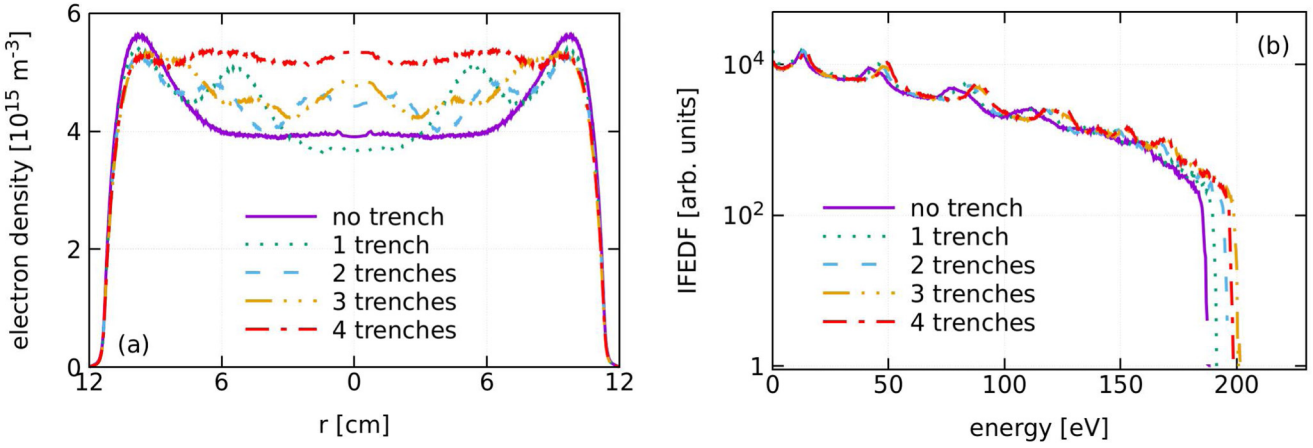

FIG. 9. Radial distributions of time averaged electron density at $z = 1$ cm (above the powered electrode) (a) and ion flux-energy distribution functions (IFEDFs) (b) at the powered electrode for reactors without trench and with 1–4 ring-shaped trenches at the grounded electrode. The other discharge conditions are the same as in Fig. 2.

IV. CONCLUSIONS

Based on 2d3v GPU accelerated PIC/MCC simulations, the electron power absorption dynamics and the radial plasma uniformity in capacitively coupled plasmas are studied in the presence of structured electrodes (having vertical trenches). Strong ionization is observed at the electrode edges due to enhanced local electron power absorption caused by edge effects. Such effects lead to non-uniformities of the plasma density, i.e., high density peaks are formed near the sidewall. With a trench set at the powered electrode, the plasma density at the trench orifice is strongly increased. This is caused by enhanced local electron power absorption inside and above the trench. Due to the geometrical reactor asymmetry, a large sheath is formed at the powered electrode. Electrons penetrate into such a trench during the local sheath collapse and are strongly accelerated toward the bulk region by the sheaths at the trench walls during the local sheath expansion phase within the RF period. Strong electron bounce resonance heating inside the trench results in a high mean electron energy inside such structures. At the trench orifice, the cross-firing of energetic electrons due to the expansion of curved sheaths at the trench corners in combination with high energy electrons, which are pushed out of the trench, leads to a high (local) ionization rate. By tracing the trajectories of selected electrons inside the trench, electrons are found to acquire high energies through bouncing between the sheaths at the trench walls.

In order to use the trench effects to improve the radial plasma uniformity above planar wafers, we have investigated the scenario with various numbers of trenches at the grounded counter electrode. Since the sheath at the grounded electrode is smaller, the electron power absorption inside the trenches at the grounded electrode is less pronounced compared to that in the powered electrode trench, but the electron density below the trenches is still enhanced significantly and can be made similar to the density near the reactor sidewall. With four trenches at the grounded electrode, a good plasma uniformity was achieved above the powered electrode. Moreover, with increasing the number of trenches at the grounded electrode, the geometrical asymmetry is slightly enhanced, which leads to small changes of the DC self-bias, while the IFEDF at the powered electrode was found to be almost unaffected.

Our results show that the electron power absorption and the radial plasma density profile can be controlled to a great extent by including trenches in the electrodes. Although different reactor geometries might be used in commercial CCPs, the radial nonuniformities caused by edge, standing wave, or skin effects are all expected to be compensated by structured electrodes with different trench shapes and dimensions. Thus, these results are highly relevant for applications where they can serve as a basis for plasma reactor design and knowledge based process optimization. Clearly, further investigations on the effects of various types of structured electrodes at different discharge conditions are required.

ACKNOWLEDGMENTS

This work was supported by the National Natural Science Foundation of China (NNSFC, Nos. 12020101005 and 11975067), China Scholarship Council (No. 201906060024), by the German Research Foundation in the frame of the project "Electron heating in capacitive RF plasmas based on moments of the Boltzmann equation: from fundamental understanding to knowledge based process control" (No. 428942393), and by the National Office for Research, Development and Innovation of Hungary (NKFIH) via Grant Nos. K-134462, K-132158, and FK-128924.

DATA AVAILABILITY

The data that support the findings of this study are available from the corresponding author upon reasonable request.

REFERENCES

[1]M. A. Lieberman and A. J. Lichtenberg, *Principles of Plasma Discharges and Materials Processing*, 2nd ed. (Wiley, New York, 2005).
[2]P. Chabert and N. Braithwaite, *Physics of Radio-Frequency Plasmas* (Cambridge University, Cambridge, 2011).
[3]T. Makabe and Z. L. Petrovic, *Plasma Electronics: Applications in Microelectronic Device Fabrication*, 2nd ed. (CRC, Boca Raton, FL, 2014).
[4]S. Wilczek, J. Trieschmann, J. Schulze, E. Schuengel, R. P. Brinkmann, A. Derzsi, I. Korolov, Z. Donkó, and T. Mussenbrock, Plasma Sources Sci. Technol. **24**, 024002 (2015).
[5]B. G. Heil, U. Czarnetzki, R. P. Brinkmann, and T. Mussenbrock, J. Phys. D: Appl. Phys. **41**, 165202 (2008).
[6]Z. Donkó, J. Schulze, B. G. Heil, and U. Czarnetzki, J. Phys. D: Appl. Phys. **42**, 025205 (2008).
[7]U. Czarnetzki, B. G. Heil, J. Schulze, Z. Donkó, T. Mussenbrock, and R. P. Brinkmann, J. Phys.: Conf. Ser. **162**, 012010 (2009).
[8]S. Ries, L. Banko, M. Hans, D. Primetzhofer, J. M. Schneider, A. Ludwig, P. Awakowicz, and J. Schulze, Plasma Sources Sci. Technol. **28**, 114001 (2019).
[9]J. Schulze, E. Schüngel, Z. Donkó, and U. Czarnetzki, Plasma Sources Sci. Technol. **20**, 015017 (2011).
[10]J. Schulze, E. Schüngel, Z. Donkó, and U. Czarnetzki, Plasma Sources Sci. Technol. **19**, 045028 (2010).
[11]E. Schüngel, D. Eremin, J. Schulze, T. Mussenbrock, and U. Czarnetzki, J. Appl. Phys. **112**, 053302 (2012).
[12]I. Korolov, A. Derzsi, Z. Donkó, and J. Schulze, Appl. Phys. Lett. **103**, 064102 (2013).
[13]T. Lafleur, P. A. Delattre, E. V. Johnson, and J. P. Booth, Appl. Phys. Lett. **101**, 124104 (2012).
[14]Q.-Z. Zhang, W. Jiang, L.-J. Hou, and Y.-N. Wang, J. Appl. Phys. **109**, 013308 (2011).
[15]Q.-Z. Zhang, S.-X. Zhao, W. Jiang, and Y.-N. Wang, J. Phys. D: Appl. Phys. **45**, 305203 (2012).
[16]P. Hartmann *et al.*, Plasma Sources Sci. Technol. **29**, 075014 (2020).
[17]P. Hartmann *et al.*, J. Phys. D: Appl. Phys. **54**, 255202 (2021).
[18]E. Schüngel, S. Brandt, Z. Donkó, I. Korolov, A. Derzsi, and J. Schulze, Plasma Sources Sci. Technol. **24**, 044009 (2015).
[19]T. Lafleur, Plasma Sources Sci. Technol. **25**, 013001 (2015).
[20]T. Lafleur, R. W. Boswell, and J. P. Booth, Appl. Phys. Lett. **100**, 194101 (2012).
[21]S. Brandt *et al.*, Plasma Sources Sci. Technol. **25**, 045015 (2016).
[22]P. Diomede and D. J. Economou, J. Appl. Phys. **115**, 233302 (2014).
[23]B. Bruneau, T. Novikova, T. Lafleur, J. P. Booth, and E. V. Johnson, Plasma Sources Sci. Technol. **23**, 065010 (2014).
[24]B. Bruneau, J. Wang, J.-C. Dornstetter, and E. V. Johnson, J. Appl. Phys. **115**, 084901 (2014).
[25]E. V. Johnson, T. Verbeke, J.-C. Vanel, and J.-P. Booth, J. Phys. D: Appl. Phys. **43**, 412001 (2010).
[26]E. Johnson, S. Pouliquen, P. Delattre, and J. Booth, J. Non-Cryst. Solids **358**, 1974 (2012).

[27]A. R. Gibson, A. Greb, W. G. Graham, and T. Gans, Appl. Phys. Lett. **106**, 054102 (2015).
[28]M. J. Kushner, J. Appl. Phys. **94**, 1436 (2003).
[29]S. Yang, Y. Zhang, H.-Y. Wang, S. Wang, and W. Jiang, Phys. Plasmas **24**, 033504 (2017).
[30]L. Wang, D.-Q. Wen, P. Hartmann, Z. Donkó, A. Derzsi, X.-F. Wang, Y.-H. Song, Y.-N. Wang, and J. Schulze, Plasma Sources Sci. Technol. **29**, 105004 (2020).
[31]S. You *et al.*, Thin Solid Films **519**, 6981 (2011).
[32]M. Oberberg, J. Kallähn, P. Awakowicz, and J. Schulze, Plasma Sources Sci. Technol. **27**, 105018 (2018).
[33]M. Oberberg *et al.*, Plasma Sources Sci. Technol. **29**, 075013 (2020).
[34]B. Zheng, Y. Fu, K. Wang, T. Schuelke, and Q. H. Fan, Plasma Sources Sci. Technol. **30**, 035019 (2021).
[35]M. A. Lieberman, A. J. Lichtenberg, E. Kawamura, and A. M. Marakhtanov, Plasma Sources Sci. Technol. **24**, 055011 (2015).
[36]D.-Q. Wen, E. Kawamura, M. A. Lieberman, A. J. Lichtenberg, and Y.-N. Wang, Plasma Sources Sci. Technol. **26**, 015007 (2016).
[37]D.-Q. Wen, E. Kawamura, M. A. Lieberman, A. J. Lichtenberg, and Y.-N. Wang, J. Phys. D: Appl. Phys. **50**, 495201 (2017).
[38]K. Zhao, D.-Q. Wen, Y.-X. Liu, M. A. Lieberman, D. J. Economou, and Y.-N. Wang, Phys. Rev. Lett. **122**, 185002 (2019).
[39]P. Chabert, J.-L. Raimbault, J.-M. Rax, and A. Perret, Phys. Plasmas **11**, 4081 (2004).
[40]M. A. Lieberman, J. P. Booth, P. Chabert, J. M. Rax, and M. M. Turner, Plasma Sources Sci. Technol. **11**, 283 (2002).
[41]T. Mussenbrock, T. Hemke, D. Ziegler, R. P. Brinkmann, and M. Klick, Plasma Sources Sci. Technol. **17**, 025018 (2008).
[42]C. H. Kim, H. Kim, G. Park, and H. J. Lee, Plasma Sources Sci. Technol. **30**, 065031 (2021).
[43]K. Bera, S. Rauf, K. Ramaswamy, and K. Collins, J. Vac. Sci. Technol. A **27**, 706 (2009).
[44]S. Rauf, Plasma Sources Sci. Technol. **29**, 095019 (2020).
[45]L. Bárdoš, Surf. Coat. Technol. **86–87**, 648 (1996).
[46]X.-X. Jiang, F. He, Q. Chen, T. Ge, and J.-T. Ouyang, Phys. Plasmas **21**, 033508 (2014).
[47]L. He, F. He, J. Ouyang, and W. Dou, Phys. Plasmas **27**, 123511 (2020).
[48]Y. Fu, B. Zheng, P. Zhang, Q. H. Fan, and J. P. Verboncoeur, J. Appl. Phys. **129**, 023302 (2021).
[49]K. Kutasi and Z. Donkó, J. Phys. D **33**, 1081 (2000).
[50]H. S. Lee, Y. S. Lee, S. H. Seo, and H. Y. Chang, Appl. Phys. Lett. **97**, 081503 (2010).
[51]H. Lee, Y. Lee, S. Seo, and H. Chang, Thin Solid Films **519**, 6955 (2011),
[52]H. Schmidt, L. Sansonnens, A. A. Howling, C. Hollenstein, M. Elyaakoubi, and J. P. M. Schmitt, J. Appl. Phys. **95**, 4559 (2004).
[53]S. J. Doyle, T. Lafleur, A. R. Gibson, P. Tian, M. J. Kushner, and J. Dedrick, Plasma Sources Sci. Technol. **26**, 125005 (2017).
[54]Y. Ohtsu and H. Fujita, Appl. Phys. Lett. **92**, 171501 (2008).
[55]Y. Ohtsu and Y. Kawasaki, J. Appl. Phys. **113**, 033302 (2013).
[56]Y. Ohtsu, N. Matsumoto, J. Schulze, and E. Schuengel, Phys. Plasmas **23**, 033510 (2016).
[57]Y. Ohtsu, Y. Yahata, J. Kagami, Y. Kawashimo, and T. Takeuchi, IEEE Trans. Plasma Sci. **41**, 1856 (2013).
[58]Y. Ohtsu and N. Matsumoto, J. Vac. Sci. Technol. A **32**, 031304 (2014).
[59]T. Lafleur and R. W. Boswell, Phys. Plasmas **19**, 023508 (2012).
[60]N. Schmidt, J. Schulze, E. Schüngel, and U. Czarnetzki, J. Phys. D: Appl. Phys. **46**, 505202 (2013).
[61]Y.-X. Liu, Q.-Z. Zhang, W. Jiang, L.-J. Hou, X.-Z. Jiang, W.-Q. Lu, and Y.-N. Wang, Phys. Rev. Lett. **107**, 055002 (2011).
[62]L. Wang, P. Hartmann, Z. Donko, Y.-H. Song, and J. Schulze, Plasma Sources Sci. Technol. **30**, 085011 (2021).
[63]L. Wang, P. Hartmann, Z. Donkó, Y.-H. Song, and J. Schulze, Plasma Sources Sci. Technol. **30**, 054001 (2021).
[64]D. Hegemann, M. Michlíček, N. E. Blanchard, U. Schütz, D. Lohmann, M. Vandenbossche, L. Zajíčková, and M. Drábik, Plasma Processes Polym. **13**, 279 (2016).
[65]D. Hegemann, E. Bülbül, B. Hanselmann, U. Schütz, M. Amberg, and S. Gaiser, Plasma Processes Polym. **18**, 2000176 (2020).
[66]COP database, see www.lxcat.net, retrieved on January 10, 2020.
[67]R. McEachran and A. Stauffer, Eur. Phys. J. D **68**, 153 (2014).
[68]Hayashi database, see www.lxcat.net, retrieved on January 10, 2020.
[69]M. Hayashi, "Bibliography of electron and photon cross sections with atoms and molecules published in the 20th century—Argon," Technical Report No. NIFS-DATA-072, National Institute for Fusion Science, Japan, 2003.
[70]A. V. Phelps, J. Phys. Chem. Ref. Data **20**, 557 (1991).
[71]A. V. Phelps, J. Appl. Phys. **76**, 747 (1994).
[72]Z. Donkó, Plasma Sources Sci. Technol. **20**, 024001 (2011).
[73]Z. Donkó, Phys. Rev. E **57**, 7126 (1998).
[74]A. Okhrimovskyy, A. Bogaerts, and R. Gijbels, Phys. Rev. E **65**, 037402 (2002).
[75]Y. Ohtsu and H. Urasaki, Plasma Sources Sci. Technol. **19**, 045012 (2010).